The theory of the magnon spectrum for CuO

1996 J. Phys.: Condens. Matter 8 1785

(http://iopscience.iop.org/0953-8984/8/11/021)

J. Phys.: Condens. Matter **8** (1996) 1785–1795. Printed in the UK

The theory of the magnon spectrum for CuO

B V Karpenko, A V Kuznetsov and V V Dyakin

Institute of the Physics of Metals, The Ural Department of the Academy of Science of Russia, 620219 Ekaterinburg, Russia

Received 29 August 1995, in final form 14 November 1995

Abstract. The magnon spectrum of the low-temperature antiferromagnetic commensurate phase in the monoclinic structure of the tenorite (CuO) is investigated from the theoretical point view. The energy operator consists of the exchange interactions, the magnetic anisotropy energy and the Zeeman energy. The primitive cell of the antiferromagnetic phase contains eight copper ions. In zero magnetic field the spectrum consists of four doubly degenerate branches: two acoustic and two optical branches. The magnon energy is determined by the fourth-order equation at an arbitrary quasi-impulse direction. An attempt was made to find the exchange interaction parameters and anisotropy energy by comparison of the theoretical expressions with the experimental dispersion curves for the crystallographic direction [010]. Four versions for the set of exchange parameters were obtained. All exchange integrals are negative in all cases. The exchange interactions in the (a, c) plane noticeably exceed the others.

1. Introduction

In the last few years, interest in the study of the physical properties of tenorite (CuO) has arisen in connection with the problem of high-temperature superconductivity. Although the compound CuO is not a superconductor itself, some features of its crystal structure mean that tenorite is related to the copper-containing high-temperature superconductors.

The interest in CuO is even stronger because of the indication of the existence of low-dimensional magnetism and antiferromagnetic ordering in it.

The crystal structure of tenorite was firstly determined by Tunnel *et al* [1] and Åsbrink and Norby [2].

It has been established also that CuO is antiferromagnetic. Forsyth *et al* [3], Yang *et al* [4, 5] Aïn *et al* [6] and Brown *et al* [10] have investigated the magnetic structure of tenorite.

It turned out that the tenorite antiferromagnetism is rather non-trivial. At temperatures below about 213 K, commensurate antiferromagnetic ordering is observed. Above this temperature and up to about 230 K an incommensurate antiferromagnetic phase arises. Further, at higher temperatures, the paramagnetic susceptibility does not follow the Curie–Weiss law but rises with increasing temperature and passes through a wide maximum at about 550 K [7, 8]. Such behaviour is typical of low-dimensional magnets.

Aïn *et al* [9] investigated the spin-wave excitations at low temperatures and obtained experimental dispersion curves for different crystallographic directions. In the present paper we also study the spin-wave spectrum from the theoretical point of view in the Heisenberg exchange approximation, taking into account the anisotropy and Zeeman energies.

0953-8984/96/111785+11$19.50

2. Information on the crystal and magnetic structure

The compound CuO has a crystal structure with the monoclinic space group C2/c (No. 15). The lattice parameters are [2] $a = 4.6837$ Å, $b = 3.4226$ Å, $c = 5.1288$ Å and $\beta = 99.54^\circ$. In the elementary cell containing four CuO 'molecules' the copper ions occupy the 4*c* positions 1 (1/4, 1/4, 0), 2 (3/4, 3/4, 0), 3 (1/4, 3/4, 1/2) and 4 (3/4, 1/4, 1/2), and the oxygen ions occupy the 4*e* positions 5 $(0, y, 1/4)$, 6 $(1/2, 1/2 + y, 1/4)$, 7 $(0, y, 3/4)$ and 8 $(1/2, 1/2 - y, 3/4)$, where $y = 0.4184$.

On the whole the crystal structure could be described in the following manner [2]. The structure elements are CuO_4 parallelograms. These parallelograms form chains by the side-sharing edges. Such chains traverse the crystal along the [110] and $[1\bar{1}0]$ directions. Each chain of [110] type is linked with two neighbouring chains of $[1\bar{1}0]$ by corner sharing. As a consequence, two types of the copper ion site arise: Cu(1) for $[1\bar{1}0]$ direction and Cu(2) for the [110] direction.

The copper ions are carriers of the magnetic moments. At temperatures lower than about 213 K antiferromagnetic ordering of the following type arises. There are two sublattices with right (plus) and left (minus) spins. The magnetic configuration is such that a laminar structure is realized, in which the alternation of two plus layers with two minus layers takes place. The ferromagnetic layers lay in planes of $(\boldsymbol{b}, \boldsymbol{a}+\boldsymbol{c})$ type. The antiferromagnetic axis is directed along the [010] (axis [b]).

For the magnetic structure described, the primitive cell contains eight copper ions as a basis, with their coordinates

$$\begin{aligned} &\boldsymbol{g}_1 = 0 \qquad \boldsymbol{g}_2 = (\boldsymbol{a}+\boldsymbol{b})/2 \qquad \boldsymbol{g}_3 = (\boldsymbol{a}+\boldsymbol{c})/2 \qquad \boldsymbol{g}_4 = (2\boldsymbol{a}+\boldsymbol{b}+\boldsymbol{c})/2 \\ &\boldsymbol{g}_5 = \boldsymbol{a} \qquad \boldsymbol{g}_6 = (3\boldsymbol{a}+\boldsymbol{b})/2 \qquad \boldsymbol{g}_7 = (3\boldsymbol{a}+\boldsymbol{c})/2 \qquad \boldsymbol{g}_8 = (4\boldsymbol{a}+\boldsymbol{b}+\boldsymbol{c})/2. \end{aligned} \tag{2.1}$$

The primitive cell is a parallelepiped based on the primitive translation vectors

$$\boldsymbol{t}_1 = 2\boldsymbol{a} \qquad \boldsymbol{t}_2 = \boldsymbol{b} \qquad \boldsymbol{t}_3 = \boldsymbol{a}+\boldsymbol{c}. \tag{2.2}$$

The vectors $\boldsymbol{g}_1$, $\boldsymbol{g}_2$, $\boldsymbol{g}_3$ and $\boldsymbol{g}_4$ relate to Cu ions with the right (plus) momentum orientation, and the vectors $\boldsymbol{g}_5$, $\boldsymbol{g}_6$, $\boldsymbol{g}_7$ and $\boldsymbol{g}_8$ relate to the left (minus) orientation. The vectors $\boldsymbol{g}_1$, $\boldsymbol{g}_2$, $\boldsymbol{g}_5$ and $\boldsymbol{g}_6$ give the Cu(1) positions, and the vectors $\boldsymbol{g}_3$, $\boldsymbol{g}_4$, $\boldsymbol{g}_7$ and $\boldsymbol{g}_8$ give the Cu(2) positions. The low-temperature antiferromagnetic primitive cell is displayed in figure 1.

For further calculations it is convenient to introduce the rectangular coordinate system x_1, x_2, $x_3(x, y, z)$ in which the axis $[a]$ coincides with x_2, and the axis $[b]$ coincides with x_3 (figure 2).

3. Model Hamiltonian secular equation

We assume that the magnetic behaviour of the CuO crystal is determined by Heisenberg isotropic exchange interaction of localized copper ion spins S by the anisotropy energy and Zeeman energy in external magnetic field. Thus for the crystal Hamiltonian we have

$$\hat{H} = \hat{H}^{(Ex)} + \hat{H}^{(A)} + \hat{H}^{(Zeem)}. \tag{3.1}$$

The exchange energy operator has the form

$$\hat{H}^{(Ex)} = -\sum_{\boldsymbol{m}} \sum_{\boldsymbol{n}} I(\boldsymbol{m}, \boldsymbol{n}) S(\boldsymbol{m}) S(\boldsymbol{n}) \tag{3.2}$$

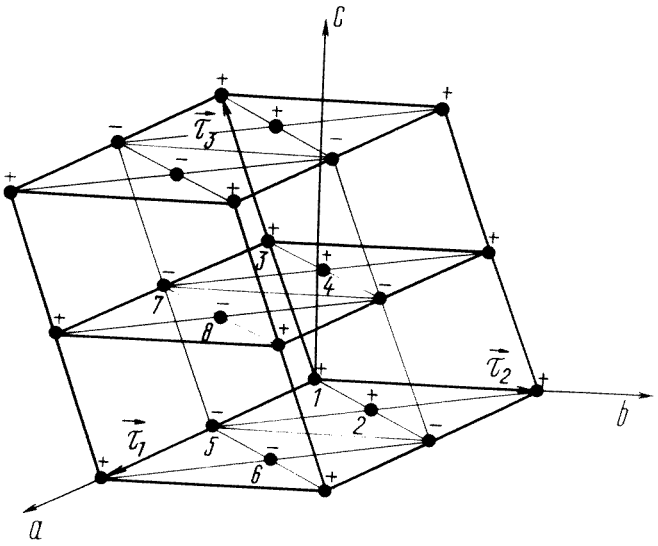

Figure 1. The primitive cell of the low-temperature antiferromagnetic phase in CuO. Only copper ions are shown. Numbers 1–8 enumerate the base ions with the vectors $\boldsymbol{g}_1$–$\boldsymbol{g}_8$ correspondingly. The signs + and − show the momentum directions. Ions Cu(1) are situated in the lower and upper (a, b) planes. Ions Cu(2) are situated in the middle (a, b) plane. The primitive cell has eight copper ions.

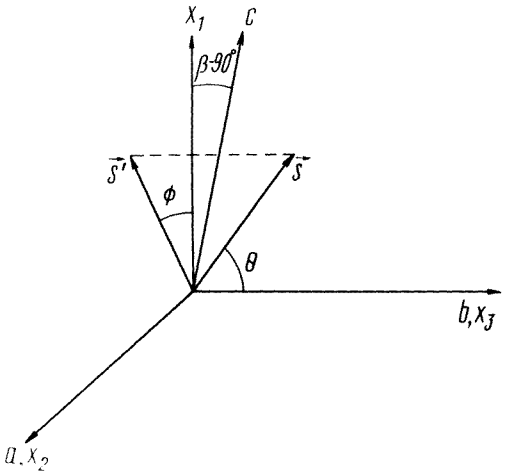

Figure 2. The crystallographic coordinate system a, b, c and rectangular coordinate system $x_1, x_2, x_3(x, y, z)$. $\boldsymbol{S}$ is the moment of any sublattice, and $\boldsymbol{S}'$ is the projection of $\boldsymbol{S}$ on the (a, c) plane. θ is the polar angle, and ϕ is the azimuthal angle.

where the summation goes over copper sublattice sites. The exchange integrals $I(\boldsymbol{m}, \boldsymbol{n})$ depend upon not only the vector difference $\boldsymbol{\Delta} = \boldsymbol{m} - \boldsymbol{n}$ but also the type of the copper

ions Cu(1) and Cu(2). Thus

$$I(\boldsymbol{m},\boldsymbol{n}) = I(\boldsymbol{\Delta}, s_m, s_n) \qquad s_m, s_n = 1, 2 \tag{3.3}$$

where the numbers s_m and s_n belong correspondingly to the vectors $\boldsymbol{m}$ and $\boldsymbol{n}$ and determine the copper ion type Cu(1) ($s = 1$) and Cu(2) ($s = 2$).

The anisotropy energy $\hat{H}^{(A)}$, which is responsible for the orientation of moments along or against the axis $[b]$, has the form

$$\hat{H}^{(A)} = -g_A \mu_B \boldsymbol{H}_A \cdot \left(\sum_{\boldsymbol{m}}^{1} \boldsymbol{S}(\boldsymbol{m}) - \sum_{\boldsymbol{m}}^{2} \boldsymbol{S}(\boldsymbol{m}) \right) \tag{3.4}$$

where the first summation goes over the first magnetic sublattice and the second summation goes over the second sublattice, g_A is the effective g-factor and μ_B is the Bohr magneton. The anisotropy field $\boldsymbol{H}_A$ is directed along the axis $[b]$ for the first magnetic sublattice and against the axis $[b]$ for the second magnetic sublattice.

The Zeeman energy has the form

$$H^{(Zeem)} = -g\mu_B \boldsymbol{S} \cdot \boldsymbol{H} \tag{3.5}$$

where g is the g-factor and $\boldsymbol{H}$ is the external magnetic field.

For further consideration it is convenient to introduce the matrix

$$I_{mn}(\boldsymbol{q}) = \sum_{\Delta} \exp(-\mathrm{i}\boldsymbol{q} \cdot \boldsymbol{\Delta}) I(\boldsymbol{\Delta}; s_m, s_n) \delta_{\boldsymbol{g}_m + \boldsymbol{\Delta}, \boldsymbol{g}_n} \qquad m, n = 1, 2, \ldots, 8 \tag{3.6}$$

where the numbers s_m, $s_n (= 1, 2)$ relate correspondingly to the vectors $\boldsymbol{g}_m$ and $\boldsymbol{g}_n$ from equations (2.1).

The matrix (3.6) has the block form

$$I_{mn}(\boldsymbol{q}) = \begin{bmatrix} I^{(1)} & I^{(2)} \\ I^{(2)} & I^{(1)} \end{bmatrix} \tag{3.7}$$

where $I^{(1)}$ and $I^{(2)}$ are 4×4 matrices:

$$I^{(1)} = \begin{bmatrix} a & b & c & d \\ b^* & a & d^* & c \\ c & d & a & e \\ d^* & c & e^* & a \end{bmatrix} \qquad I^{(2)} = \begin{bmatrix} f & b^* & g & d^* \\ b & f & d & g \\ g & d^* & f & e^* \\ d & g & e & f \end{bmatrix} \tag{3.8}$$

$$a^* = a \qquad c^* = c \qquad f^* = f \qquad g^* = g \tag{3.9}$$

$$\begin{aligned} &a = I_{11}(\boldsymbol{q}) \qquad b = I_{12}(\boldsymbol{q}) \qquad c = I_{13}(\boldsymbol{q}) \qquad d = I_{14}(\boldsymbol{q}) \\ &e = I_{34}(\boldsymbol{q}) \qquad f = I_{15}(\boldsymbol{q}) \qquad g = I_{17}(\boldsymbol{q}). \end{aligned} \tag{3.10}$$

Introducing the second quantization operators of the creation $\hat{b}^+$ and annihilation $\hat{b}$ of magnons we obtain the Hamiltonian in the form

$$\begin{aligned} \hat{H} = \Lambda + \Bigg(&\sum_{k=1}^{8} \sum_{\boldsymbol{q}} \mu_k \hat{b}^+_{g_k}(\boldsymbol{q}) \hat{b}_{g_k}(\boldsymbol{q}) + \sum_{k=1}^{8} \sum_{l=1}^{8} \sum_{\boldsymbol{q}} \nu_{kl}(\boldsymbol{q}) \hat{b}_{g_k}(\boldsymbol{q}) \hat{b}_{g_l}(-\boldsymbol{q}) \\ &+ \sum_{k=1}^{8} \sum_{l=1}^{8} \sum_{\boldsymbol{q}} \lambda_{kl}(\boldsymbol{q}) \hat{b}^+_{g_k}(\boldsymbol{q}) \hat{b}_{g_l}(\boldsymbol{q}) + Conj. \Bigg). \end{aligned} \tag{3.11}$$

The following designations are introduced into equation (3.10):

$$\begin{aligned} \Lambda = 4NS\{ &I[\sin\theta_1 \sin\theta_2 \cos(\phi_1 - \phi_2) + \cos\theta_1 \cos\theta_2]/2 \\ &- h_A(\cos\theta_1 - \cos\theta_2) - h_1(\sin\theta_1 \cos\phi_1 + \sin\theta_2 \cos\phi_2) \\ &- h_2(\sin\theta_1 \sin\phi_1 + \sin\theta_2 \sin\phi_2) - h_3(\cos\theta_1 + \cos\theta_2)\} \end{aligned} \tag{3.12}$$

where N is the number of magnetic cells in a crystal and

$$I = -4S\sum_{n} I(\boldsymbol{m},\boldsymbol{n}) \equiv -4S\sum_{n} I(0,\boldsymbol{n}). \tag{3.13}$$

Here $\boldsymbol{m}$ and $\boldsymbol{n}$ *belong to two different magnetic sublattices*. The angles θ_1, ϕ_1 and θ_2, ϕ_2, are the polar and azimuthal angles of the quantization axes for the first and second magnetic sublattices, respectively (see figure 2)

$$h_A = g_A\mu_B H_A \tag{3.14}$$

$$h_i = g\mu_B H_i \qquad i = 1,2,3 \tag{3.15}$$

$$\mu_k' = S\Bigg(\sum_{m=1}^{4} I_{lm}(0) + [\sin\theta_1\sin\theta_2\cos(\phi_1-\phi_1) + \cos\theta_1\cos\theta_2]\sum_{m=5}^{8} I_{lm}(0)\Bigg) + \cos\theta_k h_A(k)/2 + (h_1\sin\theta_k\cos\phi_k + h_2\sin\theta_k\sin\phi_k + h_3\cos\theta_k)/2 \tag{3.16}$$

where

$$\theta_k, \phi_k = \begin{cases} \theta_1, \phi_1 & \text{at } k = 1,2,3,4 \\ \theta_2, \phi_2 & \text{at } k = 5,6,7,8 \end{cases} \tag{3.17}$$

$$h_A(k) = \begin{cases} +h_A & \text{at } k = 1,2,3,4 \\ -h_A & \text{at } k = 5,6,7,8 \end{cases} \tag{3.18}$$

$$\nu_{kl}(\boldsymbol{q}) = -S\begin{bmatrix} 0 & \Phi_\nu I^{(2)*} \\ \Phi_\nu I^{(2)*} & 0 \end{bmatrix} \equiv [\nu]. \tag{3.19}$$

Here

$$\Phi_\nu = [\cos(\phi_1-\phi_2)(1-\cos\theta_1\cos\theta_2) - \sin\theta_1\sin\theta_2 + i(\cos\theta_1-\cos\theta_2)\sin(\phi_1-\phi_2)]/2 \tag{3.20}$$

$$\lambda_{kl} = -S\begin{bmatrix} I^{(1)} & \Phi_\lambda I^{(2)} \\ \Phi_\lambda^* I^{(2)} & I^{(1)} \end{bmatrix} \equiv [\lambda] \tag{3.21}$$

where

$$\Phi_\lambda = [\cos(\phi_1-\phi_2)(1+\cos\theta_1\cos\theta_2) + \sin\theta_1\sin\theta_2 - \mathrm{i}(\cos\theta_1+\cos\theta_2)\sin(\phi_1-\phi_2)]/2. \tag{3.22}$$

The equilibrium angles θ_1, ϕ_1, θ_2, ϕ_2 are determined by the conditions of extremum of the ground-state energy Λ:

$$\partial\Lambda/\partial\theta_1 = \partial\Lambda/\partial\theta_2 = \partial\Lambda/\partial\phi_1 = \partial\Lambda/\partial\phi_2 = 0. \tag{3.23}$$

The equations of motion for second quantization operators lead to the following equation for the magnon energy E:

$$\det\begin{bmatrix} A_1 & A_2^+ \\ A_2 & A_3 \end{bmatrix} = 0 \tag{3.24}$$

where

$$\begin{aligned} &A_1 = (S)^{-1}[\mu] - (2S)^{-1}E[1] + (S)^{-1}[\lambda] \\ &A_2 = (S)^{-1}[\tilde{\nu}] \qquad A_3 = (S)^{-1}[\mu] + (2S)^{-1}E[1] + (S)^{-1}[\bar{\lambda}^*]. \end{aligned} \tag{3.25}$$

Here the superscripts of the matrices have the following meanings: $+$ means Hermitian conjugation, $\sim$ means transposition, $*$ means complex conjugation and

$$\bar{\lambda}(\boldsymbol{q}) \equiv \lambda(-\boldsymbol{q}). \tag{3.26}$$

The matrix $[\mu]$ is a diagonal matrix in which the first four elements are $\mu_1 = \mu_2 = \mu_3 = \mu_4$ and the subsequent four elements are $\mu_5 = \mu_6 = \mu_7 = \mu_8$ from the equations (3.16)–(3.18).

4. The case of zero magnetic field

In zero magnetic field, equations (3.23) give

$$\theta_1 = 0 \qquad \theta_2 = \pi \qquad \phi_1 - \phi_2 = 0. \tag{4.1}$$

For the ground-state energy we have

$$\Lambda = -2NS(I + 4h_A) \tag{4.2}$$

and the minimum condition of Λ leads to the inequality

$$I + 4h_A > 0. \tag{4.3}$$

For the magnon spectrum we have

$$\Phi_\lambda = 0 \qquad \Phi_\nu = 1 \tag{4.4}$$

$$[\mu] = \mu[1] \tag{4.5}$$

where

$$\mu = S\left(\sum_{m=1}^{4} I_{lm}(0) - \sum_{m=5}^{8} I_{lm}(0)\right) + \frac{h_A}{2}. \tag{4.6}$$

Equation (3.24) reduces to

$$\det\begin{bmatrix} A & B \\ B & C \end{bmatrix} = 0 \tag{4.7}$$

$$A = \{(2S)^{-1}E - (S)^{-1}\mu\}[1] + [I^{(1)}] \qquad (4 \times 4) \tag{4.8}$$

$$B = [I^{(2)}] \qquad (4 \times 4) \tag{4.9}$$

$$C = \{-(2S)^{-1}E - (S)^{-1}\mu\}[1] + [I^{(1)}] \qquad (4 \times 4). \tag{4.10}$$

Equation (4.7) is of eighth order and gives four doubly degenerate branches of the magnon spectrum. It is possible to give the observable formulae for the magnon energies only if we consider the special directions of the magnon quasi-impulse vector $\boldsymbol{q}$.

As an example we consider the case when the vector $\boldsymbol{q}$ is directed along the $[b]$ axis. In this case, equation (4.7) gives

$$E_{1,2} = S(2)^{1/2}\{t_1 + t_1^* + p_2 + p_2^* \mp [(t_1 - t_1^* + p_2 - p_2^*)^2 + 4|t_2 + p_1|^2]^{1/2}\}^{1/2} \tag{4.11}$$

$$E_{3,4} = S(2)^{1/2}\{t_1 + t_1^* - p_2 - p_2^* \mp [(t_1 - t_1^* + p_2 + p_2^*)^2 + 4|t_2 - p_1|^2]^{1/2}\}^{1/2} \tag{4.12}$$

where

$$\begin{aligned} &t_1 = h^2 - f^2 + b^{*2} - b^2 + c^2 - g^2 \qquad t_2 = 2bh - 2fb^* + 2d(c - g) \\ &p_1 = 2hc - 2fg + 2d(b - b^*) \qquad p_2 = 2d(h - f) + 2b^*c - 2bg. \end{aligned} \tag{4.13}$$

(The equality $e = b^*$ is fulfilled in this case.) We introduced in equation (4.13) the new designation

$$h = a - \mu/S \tag{4.14}$$

where μ is determined by equation (4.6). In equations (4.11) and (4.12), $E_{1,3}$ correspond to the upper sign and $E_{2,4}$ correspond to the lower sign.

5. Comparison with experiment

Aïn *et al* [9] have found the spin-wave dispersion curves by means of inelastic neutron scattering for three crystallographic directions [101], [$\bar{1}$01] and [010]. In the present paper we make an attempt to find the exchange parameter magnitudes by comparison of the theoretical expressions obtained above with the experimental dispersion curves.

It is difficult to say beforehand how many interacting neighbours must be taken into account in order to obtain good agreement between the theory and experiment. Here we take the interactions with the neighbours up to twelfth order. Maybe, this will be sufficient as the following results will show.

Table 1 presents the neighbour coordinates, distances and corresponding exchange parameters. The lower index shows the coordination sphere number, and the upper left index indicates the exchange parameters inside the same sphere if such distinction exists. In all, 38 neighbours are taken into account.

Table 1. Table of neighbours and interactions. The first column gives the neighbourhood order N (coordination sphere number). The second column gives the number n of copper ions in the corresponding sphere. The third column gives the distance d of coordination sphere ions from the central copper ion. The fourth column gives the radius vector $\boldsymbol{\Delta}$ of the copper ion. The fifth column gives the ion type Cu(1) or Cu(2) in the pair of interactions ions. The sixth column gives the parameters of interaction I_i of coordination sphere ions with the central ion. The seventh column shows parallelism (p) or antiparallelism (a) of magnetic moments of central ion and its neighbour.

N	n	d (Å)	$\boldsymbol{\Delta}$	Cu–Cu	I_i	p, a
1	4	2.9005	$\pm(\boldsymbol{a}+\boldsymbol{b})/2$	Cu(1)–Cu(1)	${}^1I_1$	p, a
				Cu(2)–Cu(2)	${}^2I_1$	p, a
			$\pm(\boldsymbol{a}-\boldsymbol{b})/2$	Cu(1)–Cu(1)	${}^2I_1$	p, a
				Cu(2)–Cu(2)	${}^1I_1$	p, a
2	4	3.0830	$\pm(\boldsymbol{b}\pm\boldsymbol{c})/2$	Cu(1)–Cu(2)	I_2	p, a
3	2	3.1733	$\pm(\boldsymbol{a}+\boldsymbol{c})/2$	Cu(1)–Cu(2)	I_3	p
4	2	3.4226	$\pm\boldsymbol{b}$	Cu(1)–Cu(1), Cu(2)–Cu(2)	I_4	p
5	2	3.7485	$\pm(\boldsymbol{a}-\boldsymbol{c})/2$	Cu(1)–Cu(2)	I_5	a
6	4	4.6673	$\pm(\boldsymbol{a}\pm2\boldsymbol{b}+\boldsymbol{c})/2$	Cu(1)–Cu(2)	I_6	p
7	2	4.6837	$\pm\boldsymbol{a}$	Cu(1)–Cu(1), Cu(2)–Cu(2)	I_7	a
8	4	5.0759	$\pm(\boldsymbol{a}\pm2\boldsymbol{b}-\boldsymbol{c})/2$	Cu(1)–Cu(2)	I_8	a
9	2	5.1288	$\pm\boldsymbol{c}$	Cu(1)–Cu(1), Cu(2)–Cu(2)	I_9	a
10	4	5.2403	$\pm(2\boldsymbol{a}\pm\boldsymbol{b}+\boldsymbol{c})/2$	Cu(1)–Cu(2)	I_{10}	p, a
11	4	5.5440	$\pm(\boldsymbol{a}+\boldsymbol{b}+2\boldsymbol{c})/2$	Cu(1)–Cu(1)	${}^1I_{11}$	p, a
				Cu(2)–Cu(2)	${}^2I_{11}$	p, a
			$\pm(\boldsymbol{a}-\boldsymbol{b}+2\boldsymbol{c})/2$	Cu(1)–Cu(1)	${}^2I_{11}$	p, a
				Cu(2)–Cu(2)	${}^1I_{11}$	p, a
12	4	5.6428	$\pm(\boldsymbol{a}+3\boldsymbol{b})/2$	Cu(1)–Cu(1)	${}^1I_{12}$	p, a
				Cu(2)–Cu(2)	${}^2I_{12}$	p, a
			$\pm(\boldsymbol{a}-3\boldsymbol{b})/2$	Cu(1)–Cu(1)	${}^2I_{12}$	p, a
				Cu(2)–Cu(2)	${}^1I_{12}$	p, a

We treated the experimental curves [9] for the [010] direction with the help of the theoretical expressions from equations (4.11) and (4.12). When doing this, two difficulties arose. First, for directions [101], [$\bar{1}$01] and [010] we can see only two experimental curves: an acoustic curve and optical curve. However, we have, as was said above, four theoretical curves: two acoustic and two optic ones. Secondly, the existence of a large number of unknown exchange parameters raises unsurmountable mathematical problems.

The first problem was solved by assuming that the single acoustic experimental branch and single optic experimental branch each represent two merged indistinguishable branches. Automatically the second problem is removed: the number of unknown parameters diminishes.

So, equating the expressions for the two acoustic branches ($E_1 = E_3$) and two optical branches ($E_2 = E_4$) in equations (4.11) and (4.12), we obtain the relations

$$\begin{aligned} {}^1I_1 + {}^2I_{11} &= 0 \qquad {}^2I_1 + {}^1I_{11} = 0 \\ {}^1I_{12} + {}^2I_{12} &= 0 \qquad I_2 + I_{10} = 0. \end{aligned} \tag{5.1}$$

Thus, the energies of two branches become

$$E_{1,2}(\alpha) = (a_{1,2} + b_{1,2}\sin^2\alpha + c_{1,2}\sin^4\alpha)^{1/2} \tag{5.2}$$

where

$$\begin{aligned} a_1 &= (2S)^2(h_A/2S)(-4I_5 - 4I_7 - 8I_8 - 4I_9 + h_A/2S) \\ b_1 &= (2S)^2 4[(I_4 + 2I_6 - 2I_8)(-4I_5 - 4I_7 - 4I_8 - 4I_9 + h_A/2S) \\ &\quad + (I_4 + 2I_6 + 2I_8)h_A/2S)] \\ c_1 &= (2S)^2 16(I_4 + 2I_6 - 2I_8)(I_4 + 2I_6 + 2I_8) \\ a_2 &= (2S)^2(4I_3 - 4I_5 + 8I_6 - 8I_8 + h_A/2S)(4I_3 + 8I_6 - 4I_7 - 4I_9 + h_A/2S) \\ b_2 &= (2S)^2 4[(I_4 - 2I_6 + 2I_8)(4I_3 + 8I_6 - 4I_7 - 4I_9 + h_A/2S) \\ &\quad + (I_4 - 2I_6 - 2I_8)(4I_3 - 4I_5 + 8I_6 - 8I_8 + h_A/2S)] \\ c_2 &= (2S)^2 16(I_4 - 2I_6 + 2I_8)(I_4 - 2I_6 - 2I_8). \end{aligned} \tag{5.3}$$

The magnitude α changes from $-\pi/2$ to $+\pi/2$, $\alpha = \pi\zeta$, where ζ is reduced wavevector ($\boldsymbol{q} = 2\pi(0, \zeta, 0)/\tau_2$; $\tau_2 = b$; $-0.5 \leqslant \zeta \leqslant 0.5$).

The experimental optical branch is resolved well in the first six points (see figure 3), but further it almost merges with the acoustic branch. For treating the optical branch we chose the six above-mentioned points and took the seventh point on the Brillouin zone edge coinciding with the point on the acoustic curve. If one treats the optical curve only with the use of well resolved initial six points, then the coefficient c_2 has a very uncertain value because of the small change in α. We took 18 experimental points for the acoustic curve. The least-squares method gives the following values:

$$\begin{aligned} a_1 &= 8.3424 \text{ meV}^2 \qquad a_2 = 483.22 \text{ meV}^2 \\ b_1 &= 6617.0 \text{ meV}^2 \qquad b_2 = 6603.2 \text{ meV}^2 \\ c_1 &= -2394.6 \text{ meV}^2 \qquad c_2 = -2823.9 \text{ meV}^2. \end{aligned} \tag{5.4}$$

Figure 3 shows the curves calculated from equation (5.2) with the parameters from equations (5.4) together with the experimental points from [9].

So, we have *six* equations (5.3) for *seven* unknown parameters I_3, I_4, I_5, I_6, $I_7 + I_9$, I_8 and h_A. With the use of data from the paper by Kondo *et al* [11] on the magnetization and susceptibility in strong magnetic fields of tenorite powder, one can make the numerical estimation

$$h_A/I = 10^{-4}. \tag{5.5}$$

(Of course, equation (5.5) is approximate.) We use equation (5.5) as the missing seventh equation. With the help of equations (5.3)–(5.5) we obtain the exchange parameter values

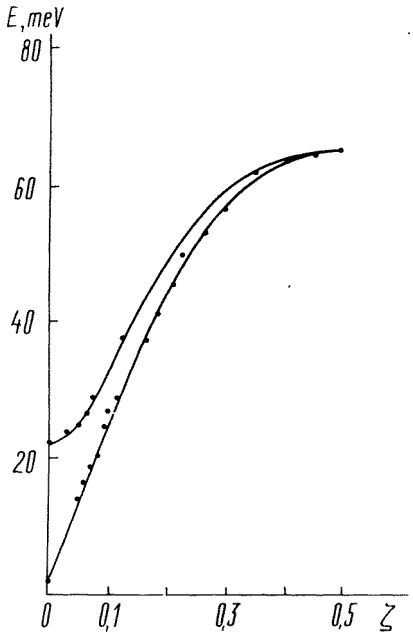

Figure 3. Dispersion curves for [010] directions: ● , experimental data from [9]; ——, calculated from equations (5.2).

which are represented in table 2. As the equation system is non-linear, we have four solutions. These solutions must be compatible with the inequality

$$Q \equiv \sum_{n}^{1} I(0, \boldsymbol{n}) - \sum_{n}^{2} I(0, \boldsymbol{n}) > 0 \tag{5.6}$$

where the first summation is over its own magnetic sublattice and the second summation is over another magnetic sublattice. In our approximation the inequality (5.6) takes the form

$$Q \equiv I_3 + I_4 - I_5 + 2I_6 - I_7 - 2I_8 - I_9 > 0. \tag{5.7}$$

Table 2. Table of exchange parameter values. The first column gives the solution number. The two last columns give the calculated values of the paramagnetic temperature Θ_N and the antiferromagnetic ordering temperature T_N for $S = 1/2$. In all cases $I = 3352$ K and $h_A = 10^{-4}I$.

Solution	$-2SI_3$ (K)	$-2SI_4$ (K)	$-2SI_5$ (K)	$-2SI_6$ (K)	$-2S(I_7 + I_9)$ (K)	$-2SI_8$ (K)	Θ_N (K)	T_N (K)
1	199	8	324	55	329	92	−1155	521
2	657	8	577	55	76	92	−1613	63
3	62	110	577	4	76	92	−1019	657
4	521	110	324	4	329	92	−1477	199

All four solutions, represented in table 2, satisfy the condition (5.7). In all cases

$$I = -8S(I_5 + I_7 + 2I_8 + I_9) = 3352 \text{ K}. \tag{5.8}$$

In table 2, the paramagnetic Néel temperature Θ_N is given. Θ_N is calculated from the formulae

$$\Theta_N = \tfrac{2}{3}S(S+1)\sum_{\boldsymbol{n}} I(0,\boldsymbol{n}) \tag{5.9}$$

which in our approximation takes the form

$$\Theta_N = \tfrac{2}{3}S(S+1)(2I_3 + 2I_4 + 2I_5 + 4I_6 + 2I_7 + 4I_8 + 2I_9). \tag{5.10}$$

Also, in table 2 the temperatures T_N of antiferromagnetic ordering are represented. The T_N-values are calculated in the molecular-field approximation:

$$T_N = \tfrac{2}{3}S(S+1)Q \tag{5.11}$$

where Q is given in equations (5.6) and (5.7). Equation (5.11) may be useless for systems with anisotropic exchange. Nevertheless, we present T_N, calculated from equation (5.11), for various orientations.

6. Discussion

So, we have obtained the equations for spin-wave energies in an arbitrary external magnetic field. Generally, there are eight spectrum branches. In zero magnetic field, four branches are realized: two acoustic and two optical branches, each being doubly degenerate.

At zero wavevector, none of the four branch energies takes a zero value. However, the natures of these energy gaps are different for the acoustic and optical branches. Therefore the acoustic and optical gaps have quite different numerical values. For the acoustic branches, the non-zero gaps are caused by the existence of the anisotropy field (besides, of course, exchange interactions) and go to zero as the anisotropy disappears in accordance with the Goldstone theorem. As for optical branches, the gap is determined dominantly by the exchange parameters only and the role of anisotropy is negligible here.

We made an attempt to find the exchange parameters values in CuO by theoretical analysis of experimental dispersion curves [9] for the [010] direction. *When doing this, the following essential assumption was made: two observed experimental curves represent two acoustic and two optical branches, which are unresolved and merged in pairs.*

Four possible versions for numerical values of exchange parameters are represented in table 2. In all four cases all exchange integrals are negative. In solution 3 the exchange parameter I_5 is the greatest, which is in accordance with the widespread point of view. However, in the remaining three cases the largest interactions are either I_3 or $I_7 + I_9$.

Generally, as displayed in table 2, the interactions I_3, I_5, $I_7 + I_9$ in the (a, c) plane summarily exceed the interplane interactions I_4, I_6 and I_8.

In order to give preference to one of the four possible solutions in table 2 it is necessary to consider some additional data. We presented in table 2 the magnitudes Θ_N and T_N, calculated from equations (5.10) and (5.11). However, this does not give much information. The experimental data for Θ_N are absent. As for T_N, the value $T_N = 199$ K in solution 4 is nearest to experiment but, as stated above, equation (5.11) is itself unreliable for our case.

In conclusion let us discuss the problem of the necessary number of neighbours. We took into account 12 coordination spheres, i.e. 38 neighbours at all. Is this too many or too few? From equations (5.3) one can see that the coefficients c_1 and c_2 are essentially *positive* magnitudes if we neglect the parameter I_8. On the other hand, the least-squares method (used for treating the experimental curve) gives quite unambiguously the *negative* sign for c_1 and c_2. So, *taking into account the interactions with neighbours from fewer than only eight coordination spheres cannot give agreement between theory and experiment in principle.*

Therefore, at least eight coordination spheres are needed to describe the dispersion curves for the [010 direction. We took into account more: 12. However, it turned out that this is almost the same as taking into account only eight spheres. Really, the interactions with tenth, eleventh and twelfth spheres are absent in the final formulae and, also, from equation (5.1) follow most probably the equalities $I_{10} = {}^{i}I_{11} = 0$ (besides the explicit equality ${}^{i}I_{12} = 0$).

As for the parameter I_9, it enters the result only in the combination $I_7 + I_9$, i.e. there is a good probability that I_9 gives only a 'correction' to I_7. So, it seems to be sufficient to take eight (or possibly nine) coordination spheres.

Attention is drawn to the fact that the interactions ${}^{i}I_1$ and I_2 of the first and second order, respectively, turned out to be negligibly small.

The authors are aware that the scalar approximation for the g-factor and the use of the Heisenberg type of exchange interaction may be serious limitations of the model.

Acknowledgments

The authors acknowledge V Ya Rayevsky and M S Dudarev for their assistance with the mathematical calculations.

References

[1] Tunnel G, Posnjak E and Ksanda C J 1935 *Z. Kristallogr.* **90** 120
[2] Åsbrink S and Norby L-J 1970 *Acta Crystallogr.* B **26** 8
[3] Forsyth J B, Brown P J and Wanklyn B M 1988 *J. Phys. C: Solid State Phys.* **21** 2917
[4] Yang B X, Tranquada J M and Shirane G 1988 *Phys. Rev.* B **38** 174
[5] Yang B X, Thurston T R, Tranquada J M and Shirane G 1988 *Phys. Rev.* B **39** 4343
[6] Aïn N, Menelle A, Wanklyn B M and Bertaut E F 1992 *J. Phys.: Condens. Matter* **4** 5327
[7] O'Keefe M and Stone F S 1962 *J. Phys. Chem. Solids* **23** 261
[8] Arbuzova T I, Samokhvalov A A, Smolyak I B, Karpenko B V, Chebotaev N M and Naumov S V 1991 *J. Magn. Magn. Mater.* **95** 168
[9] Aïn M, Reichardt W, Hennion B, Pepy G and Wanklyn B M 1989 *Physica* C **162–164** 1279
[10] Brown P J, Chattopadhyay T, Forsyth J B, Nunes V and Tasset F 1991 *J. Phys.: Condens. Matter* **3** 4281
[11] Kondo O, Ono M, Sugiura E, Sugiyama K and Date M 1988 *J. Phys. Soc. Japan* **57** 3293